Bending-shear response of self-consolidating and high-performance reinforced concrete beams

Luigi Biolzi, Sara Cattaneo *, Franco Mola

Department of Structural Engineering, Politecnico di Milano, Piazza L. da Vinci 33, 20133 Milan, Italy

Article history:
Received 11 January 2013
Revised 3 August 2013
Accepted 30 October 2013

1. Introduction

Traditional shear design procedures of reinforced concrete (RC) members are based on equations derived from the results of experimental tests [1–3], nevertheless this approach is often criticized because of its unconservativeness. In particular, experimental evidence has shown that as the size of a beam increases, the intensity of shear stress decreases, especially for lightly reinforced applications [4–6]. Therefore, a significant size effect on the shear strength, that is, for a given concrete compressive strength, the shear strength varies with the characteristic dimension of a beam, needs to be taken into account. Recently, Collins et al. [7] showed that this size effect is instigated by the reduced capability of wide cracks to transfer shear stresses, similarly to what may be detected in fiber-reinforced concrete beams [8].

The problem seems more perceptible in RC beams without stirrups whereas, with stirrups, a mitigated size dependence has been observed [6].

Among recently developed special concretes, a prominent position is attained by self-consolidating concrete (SCC), which is considered to be one of the greatest achievements in concrete technology [9–13]. The basic feature of SCC is its ability to be poured into formworks without using vibration and maintaining good stability (i.e., no segregation). Although SCC consists basically of the same components as normal vibrated concrete (NVC), its composition is quite different in order to achieve self-compacting properties. While the coarse aggregate fraction is usually limited, the powder volume is higher in a SCC. This different concrete composition leads to different mechanical properties. On one hand, the higher powder and the lower coarse aggregate content changes the granular skeleton and affects strength, modulus of elasticity and volume stability. On the other hand, in SCC there is an improvement of the grain-size distribution and of the interfacial transition zone (ITZ), which becomes denser with respect to a normal concrete [14,15].

In general, the shear strength of RC beams is supplied by different contributions such as the aggregate interlock mechanism, the compression shear zone, and the dowel action of longitudinal reinforcement [1,7,16,17]. Given the different properties of SCC in comparison to the NVC, the problem is to determine the response of RC beams under bending and shear actions [18–21].

In this paper, the shear strength of SCC RC beams with and without shear reinforcement is investigated. Four shear span–depth ratios (1.5, 2.5, 3.5 and 4.5) were considered. Overall, 16 SCC and 18 NVC beams were tested, and the outcomes of the research are compared to standard design equations. Finally, some considerations on the suitability of these equations to SCC are provided.

2. Experimental research

The experimental program involved two different groups of RC beams: in the first one, specimens were cast with NVC designed for a cubic compressive strength at 28 days, R_{ck}, of about 40, 75 and

* Corresponding author. Tel.: +39 0223994389; fax: +39 0223994220.
E-mail addresses: luigi.biolzi@polimi.it (L. Biolzi), sara.cattaneo@polimi.it (S. Cattaneo), franco.mola@polimi.it (F. Mola).

90 MPa (NVC40, NVC75, NVC90); in the second group, SCC designed for a compressive strength of about 40 MPa (SCC40) was used. The mix-design and the average compressive (R_{cm}), splitting (f_{ctsp}) and flexural (f_{cfm}) strength at the time of the tests are shown in Table 1.

The mechanical properties were determined in terms of compressive cubic strength, R_{cm} (side 150 mm), bending strength, f_{cfm} (beam 100 mm height × 100 mm width × 400 mm length), elastic modulus E_{cm}, and splitting strength, f_{ct} (cylinder diameter 150 mm, height 300 mm) according to European Standards [22–25].

High strengths were obtained by adding different mineral admixtures (fly ash and microsilica for R_{ck} equal to 75 and 90 MPa, respectively). The SCC was a powder-type obtained with limestone filler. The maximum aggregate size was 15 mm. Beams were cured in environmental condition (of about 20 °C) and covered with wet tissue (for one week).

The fresh state properties of SCC (namely workability, filling and passing ability) were evaluated with slump-flow, V-funnel, L-box, U-box and J-ring tests according to Italian Standards [26–31] and with sieve segregation tests according to European Guidelines [32]. The obtained results are shown in Table 2.

The investigation on NVC focused on beams with three different shear arm ratios:

- S: 15 × 30 × 240 cm tested with shear span a/d = 1.5;
- M: 15 × 30 × 290 cm tested with shear span a/d = 2.5;
- L: 15 × 30 × 340 cm tested with shear span a/d = 3.5.

While the investigation on SCC involved beams with four different shear arm ratios:

- S: 17 cm × 30 cm × 250 cm tested with shear span a/d = 1.5;
- M: 17 cm × 30 cm × 300 cm tested with shear span a/d = 2.5;
- L: 17 cm × 30 cm × 350 cm tested with shear span a/d = 3.5;
- XL: 17 cm×30 cm × 400 cm tested with shear span a/d = 4.5.

The effective depth of the cross section, d, was 26 cm. For each size, beams with and without stirrups (ϕ6/15 cm) were examined (two specimens of each type for SCC and one specimen of each type for NVC). Overall, 16 SCC and 18 NVC beams were tested. All specimens had the same longitudinal reinforcement (2ϕ16), while 2ϕ8 were used as compression steel in the beams with shear reinforcement. The reinforcement adopted was a grade B450C, with a yielding stress, f_y, equal to 516.5 and 589.6 MPa for NVC and SCC, respectively, and a failure strength equal to 626.5 and 660.5 MPa for NVC and SCC, respectively. The bonded length was chosen according to Eurocode 2 [33] and developed by bending the rebars at 90° to the upper part of the beam (Fig. 1). Each beam was given a proper code in order to identify all the features: namely the type of concrete (NVC40, NVC75, NVC90 or SCC40), shear reinforcement (N = none, S = stirrups), and size (S, M, L or XL). The tests on M, L and XL beams were carried out with an MTS hydraulic jack with load capability of 250 kN, while for the short specimens another MTS hydraulic jack of 1000 kN was used. The tests were displacement controlled, and the beams were monitored with at least 6 LVDTs (±5 mm range) set as shown in Fig. 1. A potentiometer (25 cm gage length) was placed on the middle section to measure the vertical displacement.

Table 1
Mix-design.

	NVC40	NVC75	NVC90	SCC40
Cement CEM II-AL 42,5 R (kg/m^3)	300	//	//	350
Cement CEM I 52,5 R (kg/m^3)	//	380	405	//
Fly ash (kg/m^3)	80	60	//	//
Microsilica in slurry al 50% (kg/m^3)	//	//	90	//
Limestone (kg/m^3)	//	//	//	160
Sand + aggregates (kg/m^3)	1870	1905	1920	1672
Naphthalene sulfonate superplasticizer (l/m^3)	4.5	//	//	//
Acrylic superplasticizer (l/m^3)	//	5.5	10	4.2
Water (l/m^3)	175	150	80	182
R_{cm} (MPa)	64.5	86.7	94.9	53.3
f_{ctsp} (MPa)	4.0	4.5	4.6	3.4
f_{cfm} (MPa)	5.90	6.55	7.05	6.95
Elastic modulus, E_{cm} (MPa)	37,400	39,200	41,500	41,000

3. Experimental results

Different behavior and failure modes were observed depending on the shear reinforcement, shear arm ratio (a/d), and type of concrete. In beams without shear reinforcement, both diagonal and bond failures were typically observed.

3.1. Bond behavior: NVC vs SCC

Bond behavior between concrete and reinforcement is a primary factor in designing reinforced concrete structures. It is well established that bond between a deformed bar and concrete depends on several parameters, such as concrete compressive and tensile strengths, confinement due to transverse reinforcement and bar geometry (diameter, shape of the ribs). Several researchers [15,21,34–39] investigated bond strength in SCC considering pull-out tests on single bars according to CEB/RILEM test method or similar, and considering different shapes of specimens (i.e. walls) to assess the so-called "top bar effect".

In the former test setup, the scatter of the experimental results is significant [11,15], with differences of the bond strength of steel in NVC and in SCC ranging between 0% and 70% [15].

Nevertheless, some studies [14,15,34] showed that the increased bond strength in SCC is due to a more uniform ITZ and a denser cement matrix.

In [35] are presented several results available in literature on pull-out tests on both NVC and SCC short anchorages in terms of ratios between bond strength and concrete compressive strength vs bar diameter.

NVC exhibited a ratio between the bond strength and the compressive strength lower than 0.4, while the results obtained on SCC, showed that, with or without confinement, the same ratio is in the range between 0.3 and 0.6. Confinement modifies the bond strength as a function of diameter: bond strength increases with bar diameter. The same trend for specimens without confinement has been observed by Lorrain and Daoud [37]; they concluded that bond strength becomes insensitive to bar diameter when pull-out failures occur. Furthermore, the SCC specimens used for the experimental research in [35] were casted with the same mix of the tested beams presented in this paper. The bond strength varied between 0.58 and 0.47 of the compressive strength (depending on the bar diameter), and the coefficient of variation varied between 0.92% and 12.23%.

Another crucial issue regarding bond in structures is the top-bar effect, a phenomenon related to bleed-water accumulation under horizontally embedded reinforcing bars. The presence of this water can locally increase the water cement ratio under the bar and weaken the bond strength.

This phenomenon is called top-bar effect because a greater reduction in bond strength occurs in the upper levels of reinforcement.

Studies on the top-bar effect have shown that properly proportioned SCC is less affected by this phenomenon than NVC [38,39].

Table 2
Properties of fresh and hardened concrete SCC40.

Slump flow (mm)	T_{500} (s)	V-funnel (s)	V-funnel – 5 min (s)	L-box (h_2/h_1)	U-box Δh (mm)	J-ring (mm)	Sieve segregation (%)
Fresh concrete							
720	0.91	4.1	6.5	0.95	5	710	14

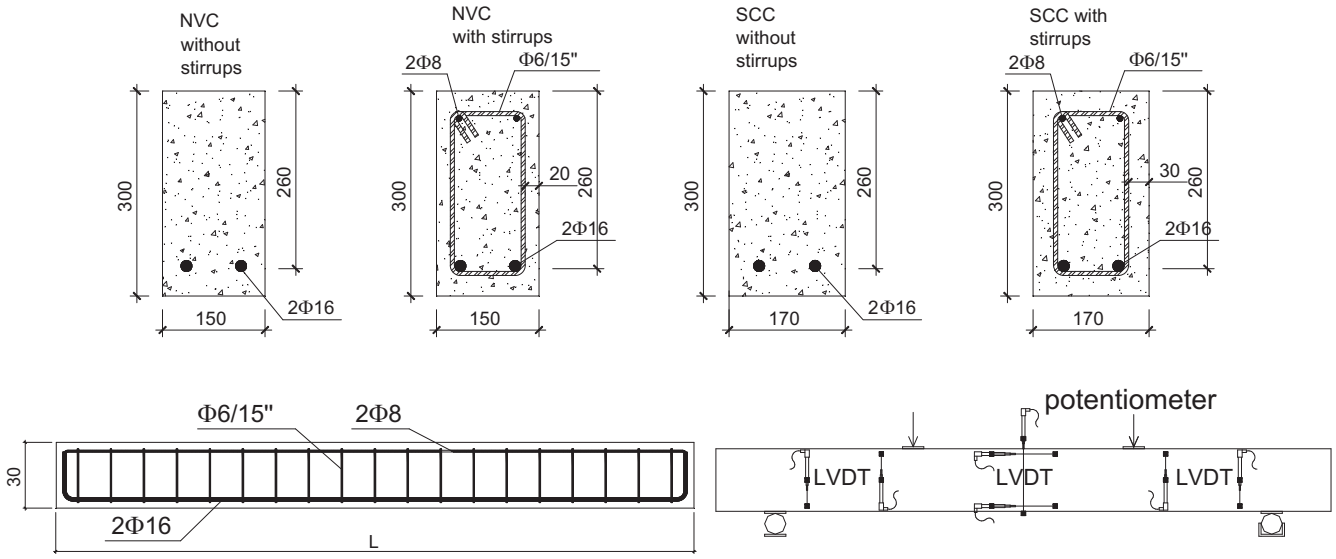

Fig. 1. Beam reinforcement, test configuration and monitoring.

The apparent increase in bond strength observed in pull-out tests and the reduced top-bar effect suggest that the bond behavior and the different microstructure of SCC can affect the structural performance of members subjected to flexure and shear and other mechanisms such as aggregate interlock and dowel action. In particular, aggregate interlock in SCC might increase due to the more dense ITZ, but it is expected to be lower with respect to ordinary concrete, because of the lower coarse aggregate content.

3.2. Beams without shear reinforcement

Beams without stirrups exhibited a brittle diagonal shear failure typically associated with bond collapse (Fig. 2b). During the tests, shear ruptures were immediately followed by bond failure. In SCC beams, the bond failure was more catastrophic and involved a large part of the anchorage length (Fig. 2b). This behavior is due to the higher bond strength observed in SCC that obviously generates higher radial pressure [40,35] which turns out in splitting failure. Short beams (a/d = 1.5) exhibited a slightly more ductile behavior with respect to the other geometries (Fig. 2a, cracks were numbered as they appear), and did not show any bond collapse. That behavior was due to the well-known arch effect, which is typical of elements with a shear arm ratio a/d lower than 2 [16,33].

An interesting behavior was observed for beams with shear arm ratio a/d = 4.5, where the two tested SCC beams failed in two different manners. One beam exhibited the typical diagonal shear collapse (specimen SCC40-N-XL-1, Fig. 2b), while the other (SCC40-N-XL-2) failed because of the crushing of the concrete in the compressive zone (Fig. 2c). This latter type of failure exhibited a ductile behavior (Fig. 8) similar to the one observed in beams with shear reinforcement.

The different failure modes could be explained by the well-known Kani's theory [16].

According to that approach, the value of the shear arm ratio a/d at which there is the transition between the failure of the concrete teeth and the flexure failure can be easily evaluated. In the present case, the theoretical a/d teeth-flexure transition is about 5 (evaluated according to Kani's theory [16]). The theoretical transition value is slightly higher than the experimental value 4.5. This could explain the different failure manner of the tested beams.

During all tests, cracks appeared between the load points (constant bending moment) at similar distance for both NVC and SCC (about 150 mm) except for one case (SCC-N-XL-2), where a reduced distance was observed due to the different type of failure. With increasing load, other cracks appeared in the regions under shear and flexure, leading to beam failure.

3.3. Beams with shear reinforcement

The beams with stirrups as shear reinforcement were characterized by a more ductile behavior. Concrete crushing in the compressive zone (Fig. 3) and a large number of cracks with branching led to a failure with detachment of a large material volume. Only short SCC beams exhibited diagonal shear failure together with stirrups collapse in SCC beams (Fig. 4).

During all tests, cracks appeared between the load points (constant bending moment) at distances of about 130 mm and 88 mm for NVC and SCC, respectively. With increasing load, other cracks appeared in the regions under shear and flexure, leading to beam failure.

4. Discussion

In Table 3, the maximum moment and the type of failure are reported for each beam, while Table 4 reports the shear strength, τ_{max}, evaluated as

$$\tau_{max} = \frac{V_{max}}{bd}, \quad (1)$$

where V_{max} is the maximum shear load, b is the beam width and d is the distance from the extreme compression fiber to the centroid of longitudinal tension reinforcement.

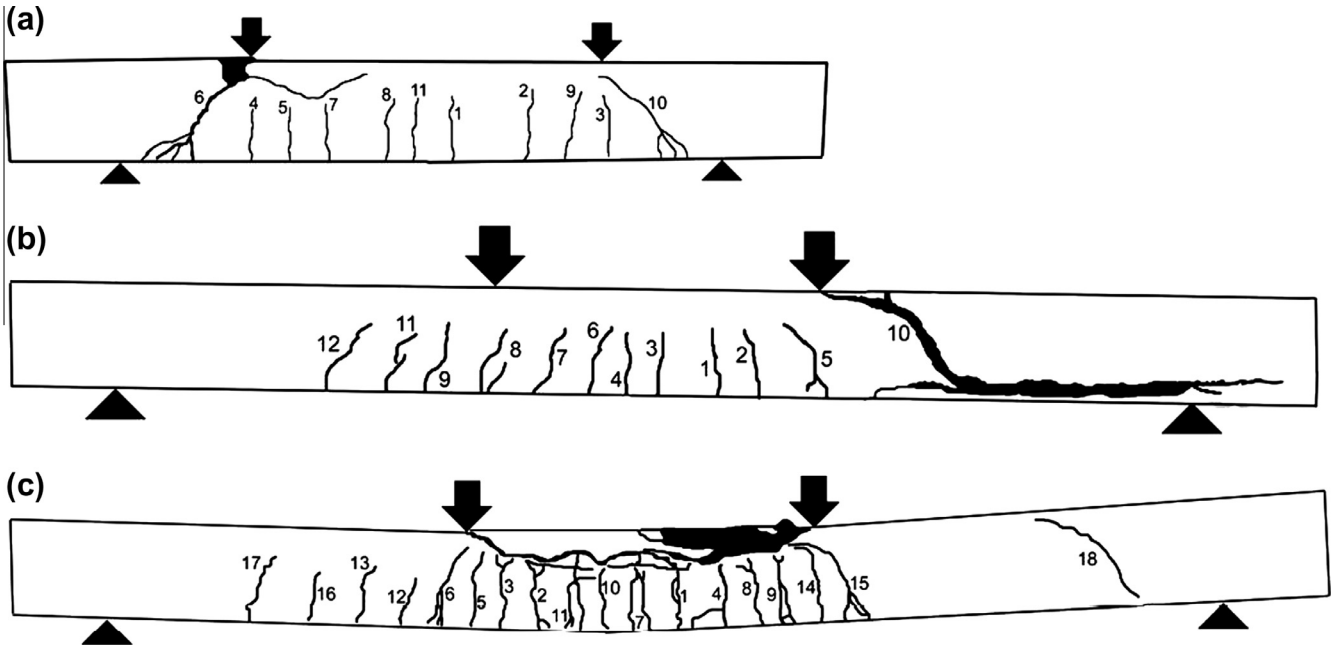

Fig. 2. Diagonal failure: short beam (SCC40-N-S) and long beam (SCC40-N-XL-1); crushing of the compressive zone) beam SCC40-N-XL-2.

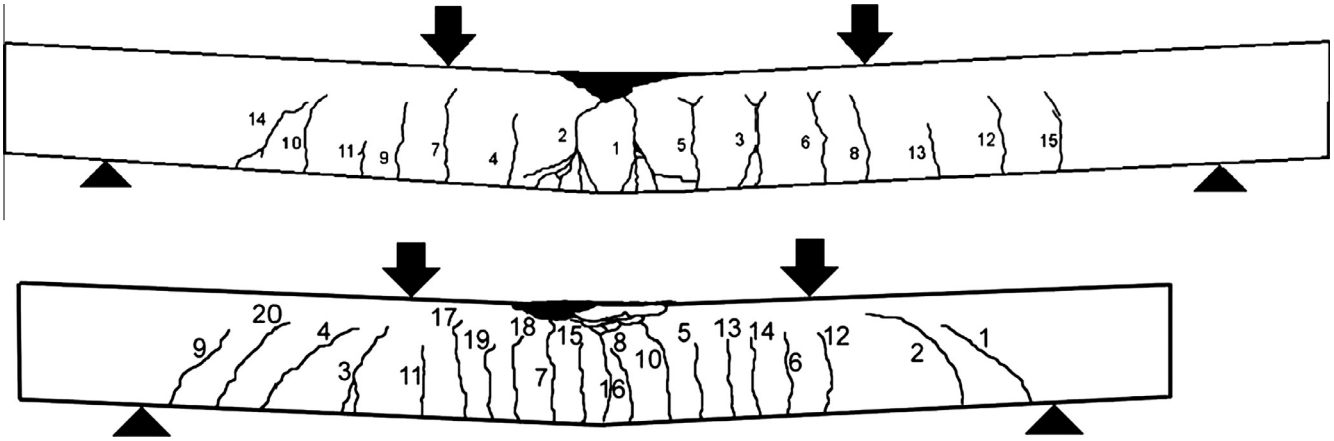

Fig. 3. Failure of beam with stirrups: crushing of the compressive zone (NVC up and SCC bottom).

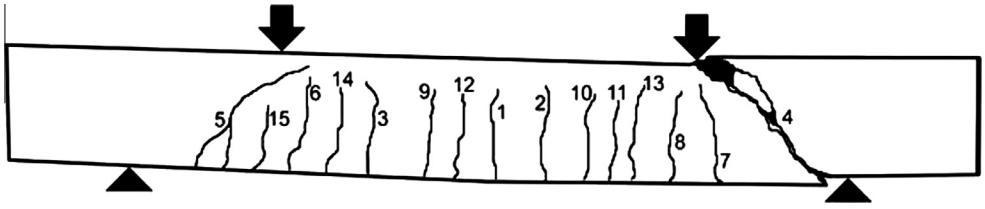

Fig. 4. Failure of short SCC beam with stirrups: diagonal and stirrups collapse.

It appears that the two considered factors (shear arm ratio *a*/*d* and shear reinforcement) significantly affect the results.

4.1. Influence of shear arm ratio a/d

Fig. 5 shows the trend of the maximum moment as a function of the shear arm ratio *a*/*d* for the considered concretes (for SCC, dots represent the single values whereas lines represent the average value). It can be observed that, for all concretes, the shear arm ratio does not significantly affect the response of shear reinforced beams, which fail due to flexure. Conversely, the beams without stirrups exhibited the typical behavior according to the Kani's valley [16,17], with a minimum moment for a shear arm ratio of 2.5. Only the beam NVC75M-N showed an anomalous behavior. In this case, the shear failure was accompanied by crushing of part of the compression chord (Fig. 6a). This second type of failure appeared after the first sudden drop (indicated with the arrow in Fig. 6b) in the moment displacement curve. The displacement control setup of the test allowed to avoid the brittle shear collapse and the development

Table 3
Maximum moment and type of failure: D (diagonal failure) – C (compressive zone crushing) – B (bond failure) – S (stirrups failure).

Beam short S	Mmax (kN m)	Failure	Beam medium M	Mmax (kN m)	Failure	Beam long L	Mmax (kN m)	Failure	Beam X-long XL	Mmax (kN m)	Failure
NVC40-S-N	50.90	D	NVC40-M-N	35.95	D + B	NVC40-L-N	37.87	D			
NVC40-S-S	53.29	C	NVC40-M-S	51.47	C	NVC40-L-S	51.25	C			
NVC75-S-N	51.78	D	NVC75-M-N	48.33	D + C	NVC75-L-N	49.96	D			
NVC75-S-S	53.33	C	NVC75-M-S	54.38	C	NVC75-L-S	53.56	C			
NVC90-S-N	54.93	D	NVC90-M-N	33.71	D	NVC90-L-N	43.52	D			
NVC90-S-S	52.31	C	NVC90-M-S	52.45	C	NVC90-L-S	52.58	C			
SCC40-S-N-1	44.42	D	SCC40-M-N-1	33.70	D + B	SCC40-L-N-1	43.03	D + B	SCC40-XL-N-1	39.83	D
SCC40-S-N-2	53.13	D	SCC40-M-N-2	31.78	D + B	SCC40-L-N-2	49.15	C	SCC40-XL-N-2	55.69	C
SCC40-S-S-1	69.05	D + S	SCC40-M-S-1	71.11	C	SCC40-L-S-1	64.04	C	SCC40-XL-S-1	62.66	C
SCC40-S-S-2	64.72	D + S	SCC40-M-S-2	68.11	C	SCC40-L-N-2	65.12	C	SCC40-XL-S-2	64.35	C

Table 4
Shear strength.

Short		Medium		Long		X-long	
Beam	τ_{max} (MPa)	Beam	τ_{max} (MPa)	Beam	τ_{max} (MPa)	Beam	τ_{max} (MPa)
NVC40-S-N	3.35	NVC40-M-N	1.42	NVC40-L-N	1.07		
NVC40-S-S	3.50	NVC40-M-S	2.03	NVC40-L-S	1.44		
NVC75-S-N	3.40	NVC75-M-N	1.91	NVC75-L-N	1.41		
NVC75-S-S	3.51	NVC75-M-S	2.15	NVC75-L-S	1.51		
NVC90-S-N	3.61	NVC90-M-N	1.33	NVC90-L-N	1.23		
NVC90-S-S	3.44	NVC90-M-S	2.07	NVC90-L-S	1.48		
SCC40-S-N-1	2.58	SCC40-M-N-1	1.17	SCC40-L-N-1	1.07	SCC40-XL-N-1	0.77
SCC40-S-N-2	3.08	SCC40-M-N-2	1.11	SCC40-L-N-2	1.22	SCC40-XL-N-2	1.08
SCC40-S-S-1	4.01	SCC40-M-S-1	2.48	SCC40-L-S-1	1.59	SCC40-XL-S-1	1.21
SCC40-S-S-2	3.75	SCC40-M-S-2	2.37	SCC40-L-N-2	1.62	SCC40-XL-S-2	1.24

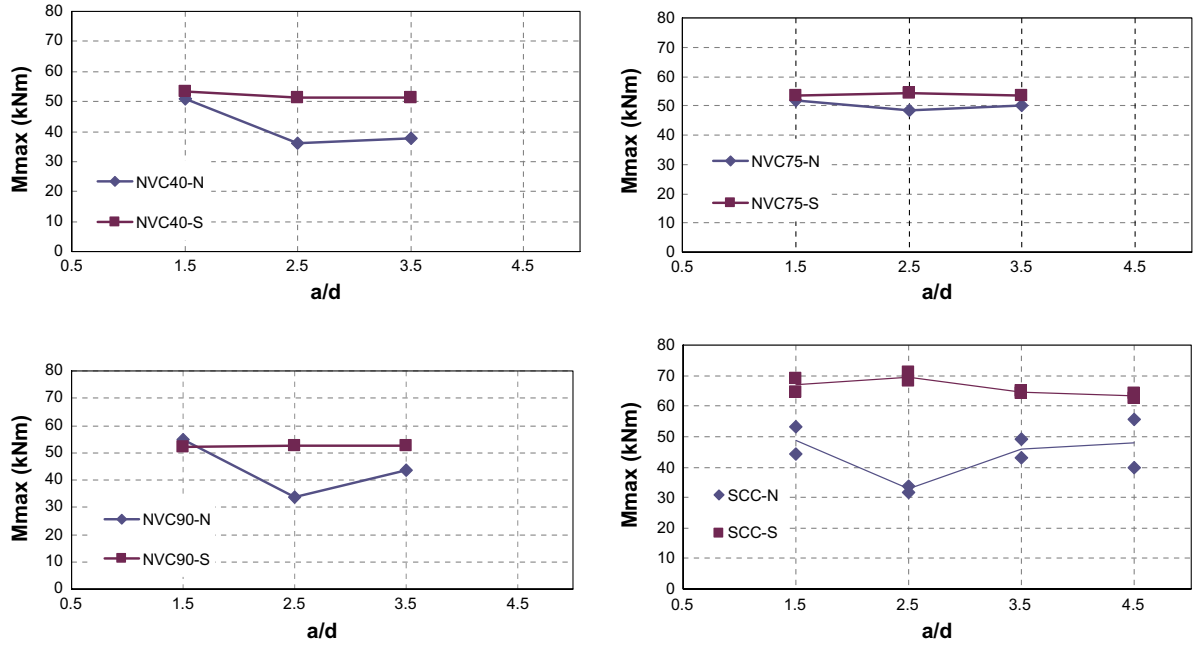

Fig. 5. Maximum moment as a function of the shear arm ratio a/d.

of another failure mechanism which involved a concrete crushing in the compression chord.

Short beams always led to a higher moment due to the arch action. However, while in NVC beams the maximum moment was similar to the one obtained for shear reinforced beams, only about 73% of the maximum moment of the corresponding shear reinforced beams was reached in the SCC case. Specifically, the experimental evidence suggests that SCC beams reached lower strength and shear reinforced SCC beams exhibited a very high shear strength (Table 4) associated with both diagonal and stirrups failure.

To compare the behavior of the different types of beam and to take into account the different concrete characteristics, f_c, beam widths, b, and yielding strength, f_{yd}, it could be useful to evaluate the normalized shear strength calculated as:

$$\tau_{nn} = \frac{V_{max}}{bd\sqrt{f_c}} \tag{2a}$$

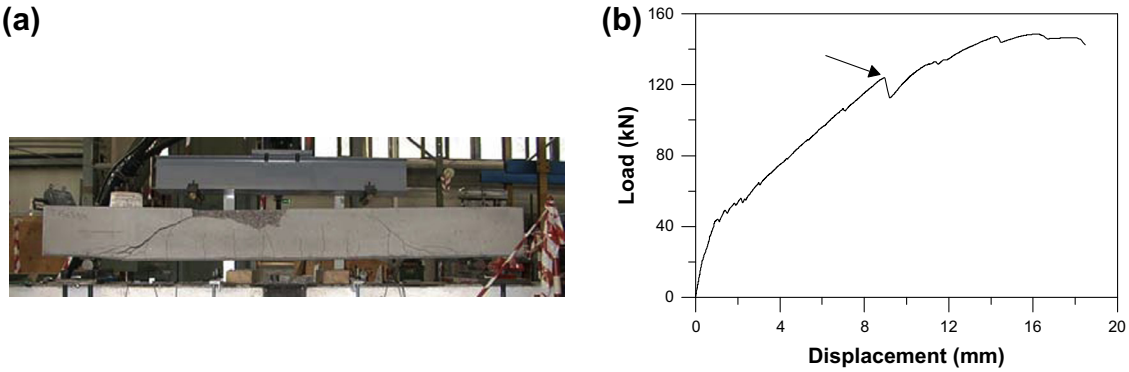

Fig. 6. (a) Failure of beam NVC75M-N and (b) load–displacement curve.

$$\tau_{ns} = \frac{V_{\max}}{bdf_{yd}\sqrt{f_c}} \tag{2b}$$

for beams without shear reinforcement and for beams with shear reinforcement, respectively. Concrete characteristics are based on the ACI 318 [41] provisions, where $\sqrt{f_c}$ is used instead of $f_c^{1/3}$, as per Eurocode 2 (EC2) [33]. It is noted that, despite this discrepancy, the two approaches lead to similar results. Fig. 7 shows that the normalized shear strength of beams without shear reinforcement is not significantly affected by the type of concrete (although SCC and NVC90 reached lower strengths), but depends mainly on the shear arm ratio a/d. In particular, short beams exhibited a strong arch effect which significantly increased the strength, while longer beams showed a slight decrease in strength.

Similar results were found by Hassan et al.[18] and by Helincks et al. [21], who considered beams without shear reinforcement with different beam depths [18] or different shear span [21]. Hassan et al. [18] found for shallow beams similar results for NVC and SCC, while for deeper beams they found lower strength for SCC beams. Also Helincks et al. [21] found equal or lower ultimate shear strength in SCC, and as in our research lower shear capacity were measured by increasing the shear to depth ratio. This could be due to a lower content of coarse aggregate in SCC beams, as for NVC90, which could lead to a reduction of the aggregate interlock and, thus, of the shear strength.

Conversely, SCC beams with shear reinforcement attained higher normalized shear strengths with respect to NVC. For this reason SCC short beams failed by both diagonal and stirrups failures due to the high bond strength between stirrups and concrete. The differences between NVC and SCC seem to reduce by increasing the beam length. In addition, with regards to SCC beams, it can be observed that the presence of shear reinforcement allowed for a limited scatter of the results, while the absence of stirrups led to higher coefficients of variation, up to 4.6% for shear reinforced beams and up to 23% for beams without stirrups. A higher standard deviation was found for the SCC40-N-XL beams (a/d = 4.5), where the two specimens showed two different types of failure.

4.2. Influence of shear reinforcement

Moment-displacement curves at mid-span are shown in Fig. 8 (short S, a/d = 1.5, medium M, a/d = 2.5, long L, a/d = 3.5, extra long XL a/d = 4.5) for both NVC (left) and SCC (right) concretes. As already stated, shear reinforcement allows to reach the full flexural capacity of the beams which failed because of the crushing of concrete in the compressive zone, showing a ductile behavior due to yielding of the longitudinal reinforcement. Only short SCC beams exhibited a limited ductility since they failed by both diagonal and stirrups failure (Fig. 8). Short NVC beams with and without shear reinforcement showed a similar behavior regardless of the concrete strength.

Longer beams without stirrups exhibited a diagonal failure, associated in some cases with bond failure, regardless of the type of concrete. This failure was brittle and associated with lower ultimate loads.

The SCC40-XL-N-2 beam showed a different behavior, failing like beams with shear reinforcement, but with an ultimate moment of about 88% of the corresponding average load of XL beams with shear reinforcement.

The ratios between the maximum moment of beams without shear reinforcement and beams with shear reinforcement are reported in Table 5.

It could be observed that NVC short beams without stirrups reached almost their full flexural capacity, while SCC beams reached only about 73%. This is likely due to the very high strength reached by the shear reinforced SCC beams. Since for SCC beams the ratio between the ultimate load without and with stirrups is always lower with respect to NVC, regardless of the concrete grade, this trend is similar for all shear arm ratios.

4.3. Cracking behavior

Experimental evidence showed different crack onsets and crack patterns depending on concrete and beam type.

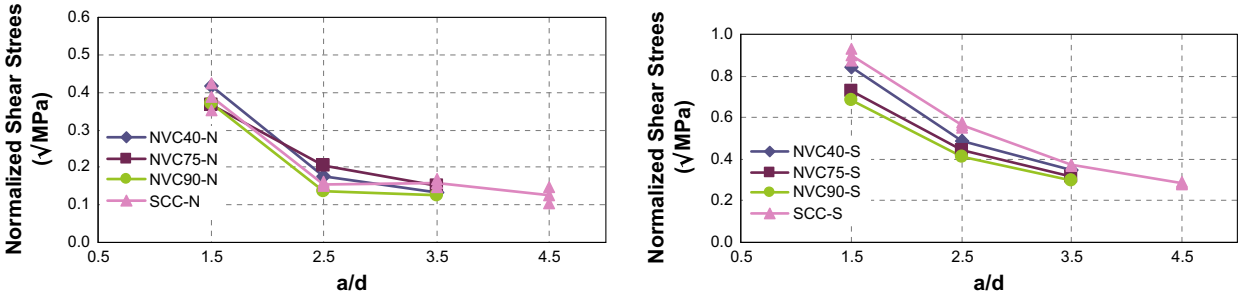

Fig. 7. Normalized shear strength – beams without (left) and with (right) shear reinforcement.

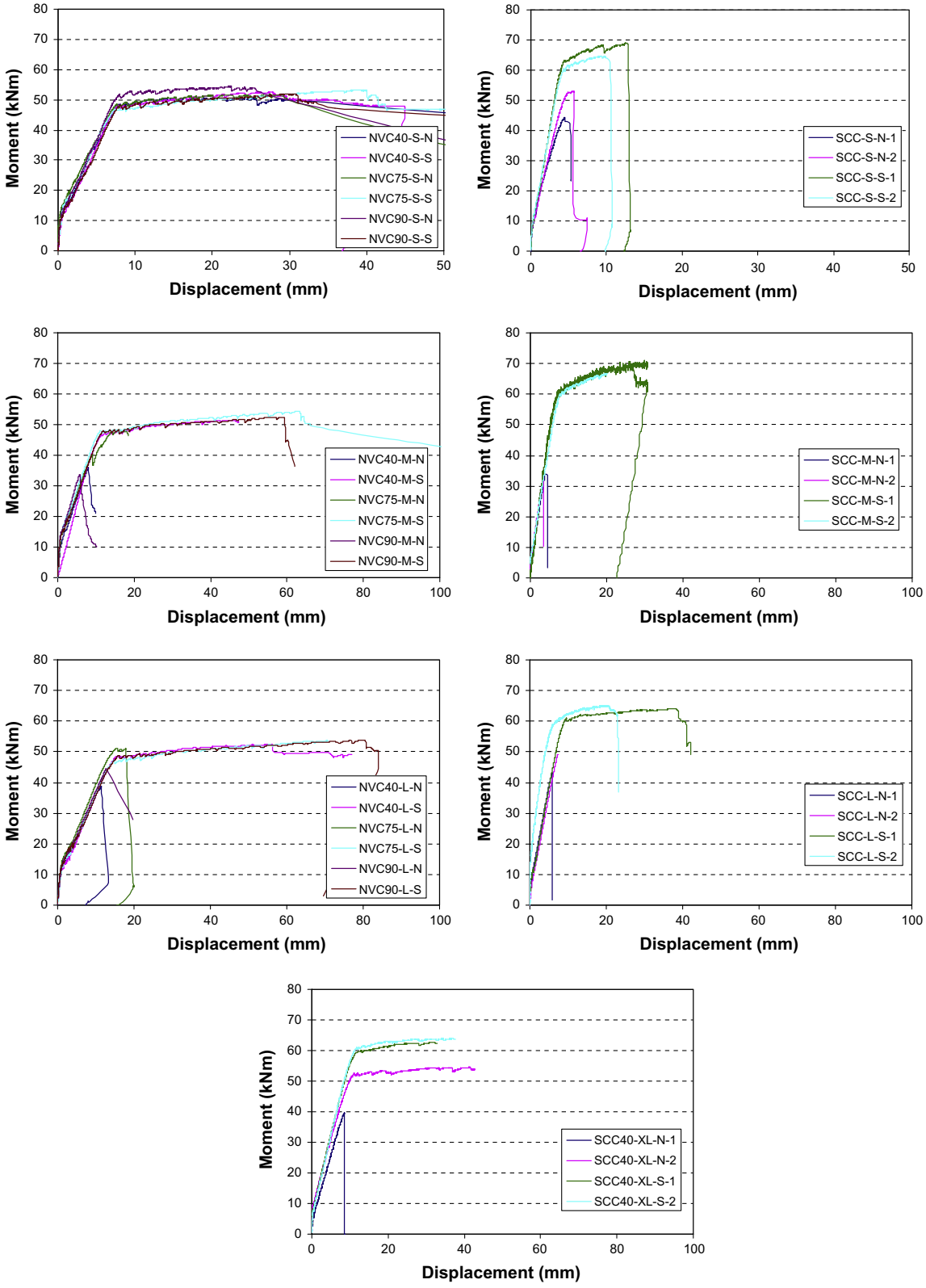

Fig. 8. Moment–displacement at midspan curves: S, M, L and XL-NVC (left) SCC (right).

Table 6 reports the average experimental and theoretical cracking moment ($M_{cr,\exp}$, $M_{cr,th}$), crack opening ($w_{\exp}$, w_{th}) and spacing ($s_{\exp}$, s_{th}).

The experimental cracking moment was visually detected and confirmed by the load–displacement curve, while its theoretical value was evaluated as:

$$M_{cr,th} = (f_{ctm,fl} - \sigma_{sh})W^*_{inf} \tag{3}$$

where $W^*_{inf} = I^*/y_{inf}$ is the section modulus of the homogenized section, $f_{ctm,fl}$ is the flexural tensile strength and σ_{sh} is the stress in the concrete due to shrinkage. The flexural tensile strength and the strain due to shrinkage were evaluated according to EC2 [33].

Table 5
Ratios between the maximum moment of beams without shear reinforcement and beams with shear reinforcement.

	Moment N/moment S			
	S	M	L	XL
NVC40	0.955	0.698	0.739	
NVC75	0.971	0.889	0.933	
NVC90	1.050	0.643	0.828	
SCC40	0.729	0.470	0.714	0.752

As shown in Fig. 9 there is good agreement between experimental and theoretical results for NVC40 and NVC75, while the scatter increases for NVC90 and, particularly, for SCC beams without shear reinforcement.

Thus, it appears that the high steel to concrete bond leads to a premature loading of the concrete and to early cracking.

The experimental crack opening and spacing (Table 6) were evaluated at a load level associated with the design moment (about 38 kN m) and taking into account only flexural cracks (in the central area of the beam subjected to a constant moment).

According to Eurocode 2 [33], the theoretical crack width w_{th} can be evaluated as

$$w_{th} = s_{th} \cdot (\varepsilon_{sm} - \varepsilon_{cm}), \tag{4}$$

where s_{th} is the maximum crack spacing, ε_{sm} and ε_{cm} are the mean strains in reinforcement and concrete, respectively, and can be evaluated as follows

$$s_{th} = k_3 c + k_1 k_2 k_4 \frac{\phi}{\rho_{p,eff}}; \quad k_3 = 3.4; \quad k_1 = 0.8 \text{ (high bond bars)};$$
$$k_2 = 0.5 \text{ (bending)}; \quad k_4 = 0.425, \tag{5}$$

$$\rho_{p,eff} = \frac{A_s}{A_{c,eff}}; \quad A_{c,eff} = b h_{c,eff} \quad h_{c,eff} = \min\left(2.5(h-d); \frac{h-x}{3}; \frac{h}{2}\right), \tag{6}$$

where c is the concrete cover, ϕ is the bar diameter, A_s the area of the steel rebars in the tension zone, d and x are the effective height of the section and the neutral axis position, respectively;

$$\varepsilon_{sm} - \varepsilon_{cm} = \frac{1}{E_s}\left[\sigma_s - \frac{k_t f_{ctm}}{\rho_{p,eff}}(1 + \alpha_e \rho_{p,eff})\right] = \frac{\sigma_s - \sigma_{s,cr}}{E_s} \geqslant 0.6\frac{\sigma_s}{E_s} \tag{7}$$

where α_e is the ratio E_s/E_{cm}, σ_s and $\sigma_{s,cr}$ are the stresses in the tension reinforcement assuming a cracked section respectively subjected to the design moment and to the cracking moment:

$$\sigma_{s,cr} = k_t \cdot f_{ctm} \cdot \frac{1}{\rho_{p,eff}}(1 + \alpha_e \rho_{p,eff}), \quad k_t = 0.6 \text{ (short-term loading)} \tag{8}$$

Beams without shear reinforcement showed a similar crack pattern (spacing of about 150 mm) for both SCC and NVC, while shear reinforced beams showed a quite different spacing (of about 150 mm for NVC and 92 mm for SCC), although the stirrup spacing was the same. Similar results were found by other authors for shear reinforced beams [20] and for unreinforced beams [19]. For all cases, the theoretical spacing is quite larger compared to its experimental value, suggesting that a review of the prediction equation is needed.

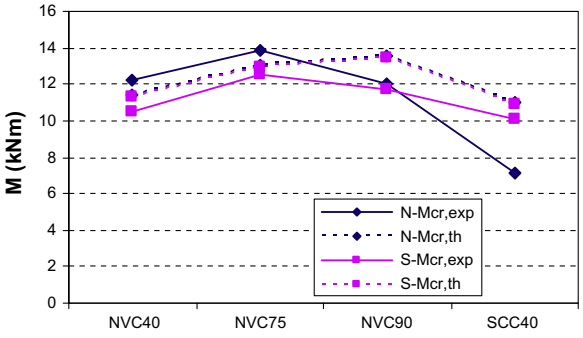

Fig. 9. Experimental and theoretical cracking moment.

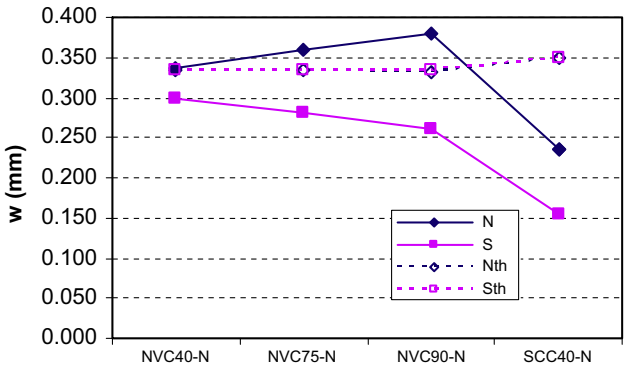

Fig. 10. Experimental and theoretical crack opening.

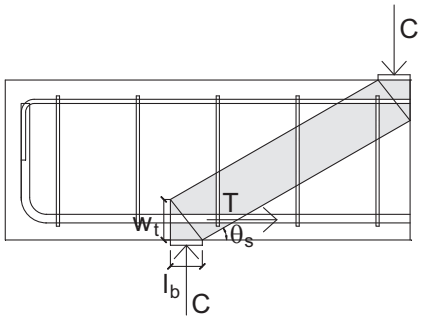

Fig. 11. Strut and tie model for short beam (ACI [41]).

Table 6
Experimental and theoretical cracking moment, crack opening and spacing.

		$M_{cr,exp}$ (kN m)	$M_{cr,th}$ (kN m)	w_{exp} (mm)	w_{th} (mm)	s_{exp} (mm)	s_{th} (mm)
N	NVC40	12.22	11.39	0.301	0.334	148.5	212.9
	NVC75	13.89	13.04	0.388	0.333	162.2	213.7
	NVC90	12.04	13.55	0.446	0.332	148.6	214.0
	SCC40	7.16	11.00	0.235	0.350	149.0	223.9
S	NVC40	10.51	11.30	0.223	0.333	168.4	212.9
	NVC75	12.51	12.94	0.282	0.333	148.6	213.7
	NVC90	11.75	13.44	0.260	0.335	142.4	214.0
	SCC40	10.10	10.93	0.155	0.350	92.6	223.9

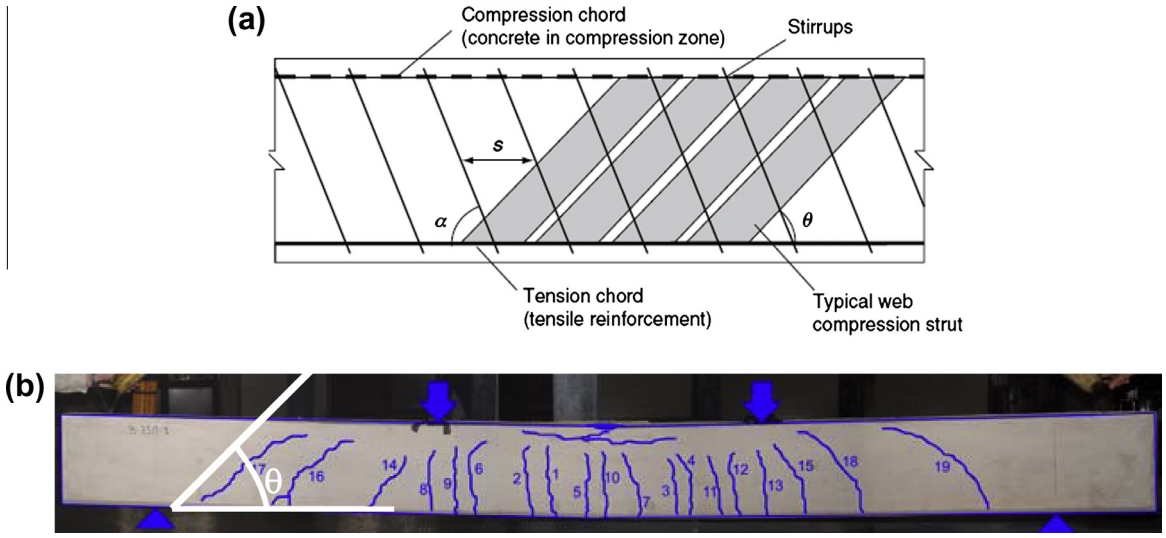

Fig. 12. Truss model analysis (EC2 [33]) for shear (a) and experimental evidence (b).

Table 7
Experimental and predicted shear load of beams without shear reinforcement (measure in kN).

Beam	V_{max}	$V/(a/2d)$	EC2 exp	ACI exp (Eq. (10))	ACI exp str.-tie	V_d (EC2)	V_d (ACI) (Eq. (10))	V_d (ACI) str.-tie
NVC40-S-N	130.51	97.88	26.75	51.57	207.63	24.83	36.16	157.18
NVC75-S-N	132.77	99.58	31.01	59.05	207.63	29.38	42.14	157.18
NVC90-S-N	140.85	105.63	32.44	61.57	207.63	30.89	44.13	157.18
SCC40-S-N-1	113.9	85.42	27.55	52.99	224.79	25.15	36.58	151.32
SCC40-S-N-2	136.23	102.17	27.55	52.99	224.79	25.15	36.58	151.32
NVC40-M-N	55.31		26.75	49.72		24.83	34.78	
NVC75-M-N	74.35		31.01	57.2		29.38	40.75	
NVC90-M-N	51.86		32.44	59.72		30.89	42.74	
SCC40-M-N-1	51.85		27.55	51.14		25.15	35.19	
SCC40-M-N-2	48.89		27.55	51.14		25.15	35.19	
NVC40-L-N	41.62		26.75	48.93		24.83	34.18	
NVC75-L-N	54.9		31.01	56.41		29.38	40.16	
NVC90-L-N	47.82		32.44	58.93		30.89	42.15	
SCC40-L-N-1	47.29		27.55	50.35		25.15	34.6	
SCC40-L-N-2	54.01		27.55	50.35		25.15	34.6	
SCC40-XL-N-1	34.04		27.55	49.91		25.15	34.27	
SCC40-XL-N-2	47.6		27.55	49.91		25.15	34.27	

Table 8
Experimental and predicted shear load of shear reinforced beams (measure in kN).

Beam	m	EC2 exp		ACI exp (Eqs. (9))	ACI exp str.-tie	V_d (EC2)		V_d (ACI) (Eqs. (9))	V_d (ACI) str.-tie
		$\cot\theta = 2.5$	$\cot\theta = 1$			$\cot\theta = 2.5$	$\cot\theta = 1$		
NVC40-S-S	136.64	113.85	45.54	102.17	207.63	86.19	34.47	64.89	157.18
NVC75-S-S	136.74	113.85	45.54	109.65	207.63	86.19	34.47	70.87	157.18
NVC90-S-S	134.13	113.85	45.54	112.17	207.63	86.19	34.47	72.86	157.18
SCC40-S-S-1	177.05	129.96	51.99	110.75	224.79	86.19	34.47	65.31	151.32
SCC40-S-S-2	165.95	129.96	51.99	110.75	224.79	86.19	34.47	65.31	151.32
NVC40-M-S	79.18	113.85	45.54	100.32		86.19	34.47	63.5	
NVC75-M-S	83.66	113.85	45.54	107.81		86.19	34.47	69.48	
NVC90-M-S	80.69	113.85	45.54	110.32		86.19	34.47	71.47	
SCC40-M-S-1	109.4	129.96	51.99	108.9		86.19	34.47	63.92	
SCC40-M-S-2	104.78	129.96	51.99	108.9		86.19	34.47	63.92	
NVC40-L-S	56.32	113.85	45.54	99.53		86.19	34.47	62.91	
NVC75-L-S	58.86	113.85	45.54	107.01		86.19	34.47	68.89	
NVC90-L-S	57.78	113.85	45.54	109.53		86.19	34.47	70.88	
SCC40-L-S-1	70.37	129.96	51.99	108.11		86.19	34.47	63.33	
SCC40-L-N-2	71.56	129.96	51.99	108.11		86.19	34.47	63.33	
SCC40-XL-S-1	53.56	129.96	51.99	107.67		86.19	34.47	63	
SCC40-XL-S-2	55	129.96	51.99	107.67		86.19	34.47	63	

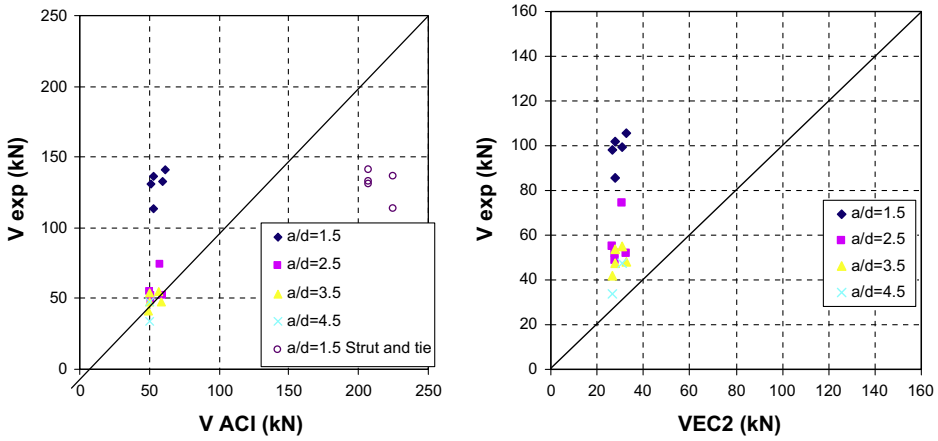

Fig. 13. Predicted shear load vs experimental shear loads: beams without shear reinforcement.

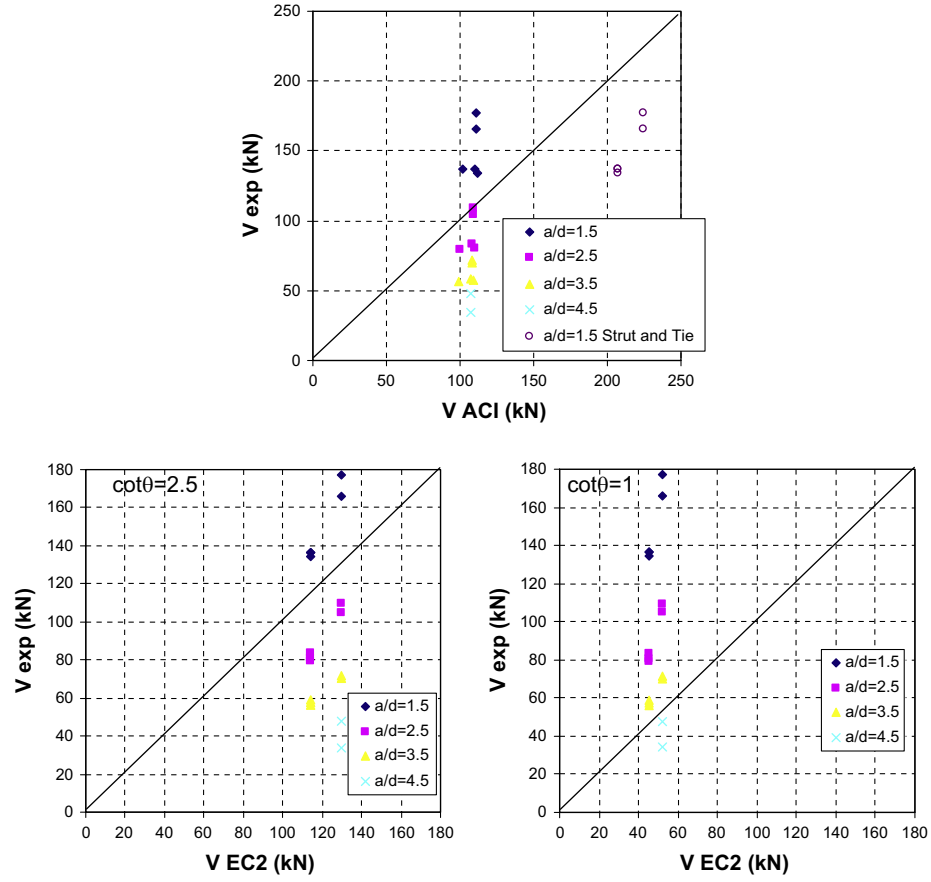

Fig. 14. Predicted shear load vs experimental shear loads: beams with shear reinforcement.

For NVC90 and SCC40 there is a significant difference between the experimental and the predicted crack opening (Fig. 10). In particular, SCC40 shows smaller crack opening and spacing due to effect of the increased steel to concrete bond for this type of concrete.

5. Comparison with design codes

The ultimate shear load was evaluated for all beams according to the provisions of ACI 318 [41] and Eurocode 2 [33].

According to ACI [41], the shear strength is:

$$V_{ACI} = \phi V_n \tag{9a}$$

where

$$V_n = V_{cACI} + V_{sACI} \tag{9b}$$

is the sum of concrete and reinforcement contributions (the second one only for shear reinforced beams).

ϕ is the strength reduction factors equal to 0.75 for member subjected to shear and torsion.

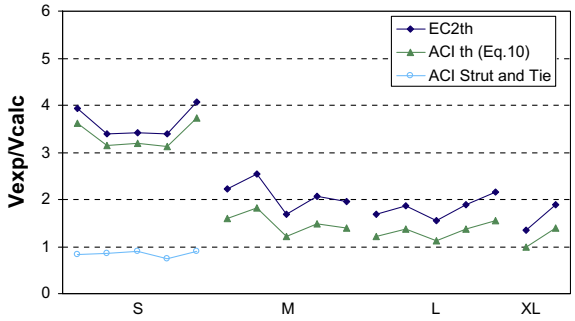

Fig. 15. Experimental shear load/design shear load: beams without shear reinforcement.

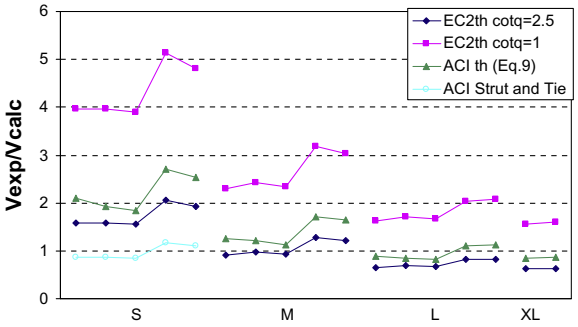

Fig. 16. Experimental shear load/design shear load: beams with shear reinforcement.

The concrete contribution is given by

$$V_{cACI} = 0.158\sqrt{f_c}bd + 17.24\rho_w \frac{V_f d}{M_f} bd \leqslant 0.29\sqrt{f_c}bd \tag{10}$$

where $\rho_w = A_s/bd$, A_s is the area of the longitudinal reinforcement, V_f and M_f are the factored shear force and moment at section. The resistance provided by shear reinforcement is given by:

$$V_{sACI} = \frac{A_{sw}}{s} d f_{yd}. \tag{11}$$

where A_{sw} is the area of the shear reinforcement and s the spacing.

According to ACI [41] short beams should be treated as deep beams because a concentrated load is applied within a distance 2 h from the face of the support. In this case Eqs. (9) should be replaced by a strut and tie model. This approach is suitable to predict the behavior in D-regions (disturbed or discontinuity region, where the Bernoulli's hypothesis of plane sections is no longer valid). For the geometry of the considered beams (Fig. 11) a CCT (Compression, Compression, Tension) node should be studied, with an inclination θ_s of the strut of about 30°, a width of the bearing ℓ_b equal to 60 mm and an effective height of the tie w_t of 76 mm.

EC2 [33] has different approaches for beams with/without shear reinforcement:

$$V_{EC2} = \left(\frac{0.18}{\gamma_c}\left(1 + \sqrt{\frac{200}{d}}\right)(100\rho_w f_c)^{1/3}\right) bd \leqslant \left(0.035\left(1 + \sqrt{\frac{200}{d}}\right)^{3/2}\sqrt{f_c}\right) bd \tag{12}$$

for beams without shear reinforcement, where γ_c is the partial safety factor (equal to 1.5). In addition, EC2 applies a reduction factor to the load, $\beta = a/2d$, for short beams (load applied at $0.5d \leqslant a \leqslant 2d$).

For beams with shear reinforcement the shear strength is given by the lower value between:

$$V_{sEC2} = \frac{A_{sw}}{s} z f_{yd} \cot\vartheta \tag{13a}$$

and

$$V_{Rd,\max} = \alpha_{cw} b z \nu_1 f_{cd} / (\cot\vartheta + \tan\vartheta) \tag{13b}$$

where z can be assumed as $0.9d$, ϑ is the angle between the concrete compression strut and the beam axis perpendicular to the shear force ($1 \leqslant \cot\vartheta \leqslant 2.5$) (where ϑ represents the inclination of the compression strut of the trussed framework model, Fig. 12), and $\nu_1 = 0.6(1 - \frac{f_{ck}}{250})$ (f_{ck} in MPa), $\alpha_{cw} = 1$ for non-compressed members.

Tables 7 and 8 report the experimental shear loads and the predictions based on EC2 [33] and ACI [41] equations, assuming the actual strength of the material (exp) and the design strength (V_d), for beams without (Table 7) and with (Table 8) shear reinforcement. For short beams the results considering both Eqs. (9) and the Strut and Tie model (ACI [41]) are reported.

By comparing the experimental and the predicted peak loads (evaluated with the material actual strength), it appears that both ACI [41] (Eqs. (9)) and EC2 [33] underestimate the strength of short beams (Fig. 13). In particular, although ACI [41] takes into account the length of the beams (by means of the V_{fd}/M_f factor), EC2 [33] provisions appear to be more effective for short beams, where the β reduction factor is applied to the shear load. Conversely, the ACI strut and tie model overestimate the shear load. According to this approach the ultimate load is due to the tie failure for NVC and for the strut failure for SCC beams.

By increasing the beam length, the safety factor reduces and, in turn, ACI [41] becomes less conservative than EC2 [33].

The same trend is observed for shear reinforced beams (Fig. 14). According to EC2 the theoretical value of the angle ϑ is lower than 21° ($\cot\vartheta = 2.5$), while experiments have shown values of about 45°. Using the first assumption, EC2 [33] overestimates (except for short beams) the shear resistance, while by assuming $\cot\vartheta = 1$, results become unconservative only for longer beams.

Considering the design shear load for beams without stirrups, both EC2 [33] and ACI [41] (Eqs. (9)) provide reasonable predictions for longer beams and are largely conservative (by a factor of 3) for short beams (Fig. 15), except by considering ACI [41] strut and tie model (by a factor of about 0.85).

The design shear values of beams with shear reinforcement assessed with ACI [41] (Eqs. (9)) and EC2 [33] are poor when the theoretical angle $\theta = 21.6°$, except for short beams. If $\theta = 45°$ (Fig. 12) is used, the design values become very conservative (Fig. 16). The strut and tie model is fairly safe (by a factor of about 1.15) only for SCC beams, while it is unsafe for NVC beams. In all cases the high compressive strength of the NVC led to a very high load carrying capacity of the strut. For this reason the tie was the weakest part of the node for NVC beams. Nevertheless, it seems that the ACI strut and tie model is not suitable for the considered beams so further analysis with others approaches could be considered [7,42–44].

6. Conclusions

An experimental investigation of the behavior of normal vibrated concrete and self-compacting concrete beams subjected to shear and flexure is presented. Test variables, which are adopted as major factors, are type of concrete (NVC and SCC), concrete compressive strength, shear arm ratio and incorporation of web reinforcement (stirrups).

Overall 34 beams were tested (18 NVC and 16 SCC), with shear arm ratios values of 1.5, 2.5, 3.5 and 4.5.

From the study, the following conclusions may be drawn.

Without shear reinforcement, a brittle behavior due to diagonal failures usually associated with bond collapse was observed.

The normalized shear strength of beams without shear reinforcement is not significantly affected by the type of concrete, but depends mainly on the shear arm ratio. However, SCC and NVC90 reached lower strength, probably due to the lower content of coarse aggregate, which leads to a reduction of the aggregate interlock and, thus, of the shear strength.

Beams without stirrups with a shear arm ratio equal to $a/d = 4.5$ showed different types of failure, suggesting that ratio could be the threshold between the "comb" and the flexural behavior.

NVC short beams ($a/d = 1.5$) without stirrups exhibited a ductile behavior similar to that observed in beams with stirrups.

SCC beams with stirrups reached very high shear strength both associated with diagonal and stirrups failure, probably due to the higher steel to concrete bond of SCC.

The differences between NVC and SCC shear reinforced beams seem to be reduced by increasing the beam length.

Beams with shear reinforcement failed due to crushing of the compressive zone in a ductile manner, showing the yielding of the longitudinal reinforcement.

Beams without shear reinforcement showed a similar crack pattern for both SCC and NVC, while shear reinforced SCC beams exhibited reduced crack spacing. The predicted crack opening for SCC40 and NVC90 is quite larger than its experimental value, probably due to the higher bond of these concretes.

It appears that code provisions cannot be simply extended to SCC, whereas a calibration of coefficients used in numerical predictions is required.

Code provisions are too conservative for short beams, except when strut and tie model is used, while they appear unconservative for longer beams. Proper strut and tie models should be studied for this type of concretes.

References

[1] Fenwick RC, Paulay T. Mechanisms of shear resistance of concrete beams. ASCE J Struct Div 1984;94(10):2325–50.

[2] Russo G, Zingone G, Puleri G. Flexure-shear interaction model for longitudinally reinforced beams. ACI Struct J 1991;88(1):60–8.

[3] Cattaneo S, Giussani F, Mola F. Flexural behavior of reinforced, prestressed and composite self-consolidating concrete beams. Constr Build Mater 2012;36:826–37.

[4] Bazant ZP, Kim PJK. Size effect in shear failure of longitudinally reinforced beams. ACI Struct J 1984;81(5):456–68.

[5] Bazant ZP, Kazemi MT. Size effect on diagonal shear failure of beams without stirrups. ACI Struct J 1991;88(3):268–76.

[6] Yu Q, Bažant ZP. Can stirrups suppress size effect on shear strength of RC beams? ASCE J Struct Eng 2011;137(5):607–17.

[7] Collins MP, Bentz EC, Sherwood EG, Xie L. An adequate theory of shear strength of reinforced concrete structure. Mag Concr Res 2008;60(9):635–50.

[8] Biolzi L, Cattaneo S, Guerrini GL. Fracture of plain and fiber reinforced concrete slabs with EA and ESPI monitoring. Appl Comp Mater 2000;7(1):1–12.

[9] Okamura H, Ouchi M. Self-compacting high performance concrete. Prog Struct Eng Mater 1998;I(4):378–83.

[10] Domone PL. Self-compacting concrete: an analysis of 11 years of case studies. Cem Concr Compos 2006;28:197–208.

[11] Domone PL. A review of the hardened mechanical properties of self-compacting concrete. Cem Concr Compos 2007;29:1–12.

[12] Walraven J. Structural aspects of self compacting concrete. In: 3rd Int RILEM symp on self compacting concrete, Reykjavik, Iceland; 2003. p. 15–22.

[13] Cattaneo S, Mola F. Assessing the quality control of self consolidating concrete properties. ASCE J Constr Eng Manage 2012;138(2):2012. http://dx.doi.org/10.1061/(ASCE)CO.1943-7862.0000410.

[14] Tragardh J. Microstructural features and related properties of self-compacting concrete. In: Proc of the first int RILEM symp; 1999. p. 175–86.

[15] Collepardi M, Borsoi A, Collepardi S, Troli R. Strength, shrinkage and creep of scc and flowing concrete. In: Proc of SCC 2005 conf center for advanced cement based materials, Northwestern University, USA; 2005. p. 911–20.

[16] Kani GNJ. Riddle of shear failure and its solution. ACI J 1964;61(4):441–67.

[17] Kani GNJ. Basics facts concerning shear failure. ACI J 1966;63(6):675–92.

[18] Hassan AAA, Hossain KMA, Lachemi M. Behaviour of full-scale self-consolidating concrete beams in shear. Cem Concr Compos 2008;30:588–96.

[19] Hassan AAA, Hossain KMA, Lachemi M. Structural assessment of corroded self-consolidating concrete beams. Eng Struct 2010;32:874–85.

[20] Sonebi M, Tamini AK, Bartos PJM. Performance and cracking behavior of reinforced beams cast with self-consolidating concrete. ACI Mater J 2003;100(6):492–500.

[21] Helincks P, Boel V, De Corte W, De Schutter G, Desnerck P. Structural behavior of powder type self-compacting concrete: bond performance and shear capacity. Eng Struct 2013;48:121–32.

[22] UNI EN 12390-3:2003. Testing hardened concrete – compressive strength of test specimens.

[23] UNI EN 12390-5:2002. Testing hardened concrete – flexural strength of test specimens.

[24] UNI EN 12390-6:2002. Testing hardened concrete – tensile splitting strength of test specimens.

[25] UNI 6556:1976. Tests of concretes. Determination of static modulus of elasticity in compression.

[26] UNI 11040. Self compacting concrete – specification, characteristics and checking. Milan; 2003.

[27] UNI 11041. Testing fresh self compacting concrete – determination of free flow and time flow. Milan; 2003.

[28] UNI 11042. Testing fresh self compacting concrete – determination of flow time in V-funnel. Milan; 2003.

[29] UNI 11043. Testing fresh self compacting concrete – determination of confined flowability in L-shape box. Milan; 2003.

[30] UNI 11044. Testing fresh self compacting concrete – determination of confined flowability in U-shape box. Milan; 2003.

[31] UNI 11045. Testing fresh self compacting concrete – determination of confined flowability in J-ring. Milan; 2003.

[32] Self-Compacting Concrete European Project Group (SCCEPG). The European guidelines for self-compacting concrete: specification, production and use; 2005. <http://www.efnarc.org/pdf/SCCGuidelinesMay2005.pdf>.

[33] Eurocode 2. Design of concrete structures – part 1-1: general rules and rules for buildings. EN 1992-1-1; 2004. 225pp.

[34] Zhu W, Sonebi M, Bartos PJM. Bond and interfacial proprieties of reinforcement in self-compacting concrete. Mater Struct 2004;37:442–8.

[35] Cattaneo S, Rosati G. Bond between steel and self-consolidating concrete: experiments and modeling. ACI Struct J 2009;106(4):530–40.

[36] Chan Y, Chen Y, Liu Y. Development of bond strength of reinforcement steel in self-consolidating concrete. ACI Struct J 2003;100(4):490–8.

[37] Lorrain M, Daoud A. Bond in self-compacting concrete. In: Proc of RILEM int symp bond in concrete – from research to standards, Budapest; 2002. p. 529–36.

[38] Khayat KH, Manai K, Trudel A. In situ mechanical properties of wall elements cast using self-consolidating concrete. ACI Mater J 1997;94(6):491–500.

[39] Valcuende M, Parra C. Bond behaviour of reinforcement in self-compacting concretes. Constr Build Mater 2008. http://dx.doi.org/10.1016/j.conbuildmat.2008.01.007.

[40] Tepfers R. Cracking of concrete cover along anchored deformed reinforcing bars. Mag Concr Res 1979;31(106):3–12.

[41] ACI Committee 318, Building Code Requirements for Structural Concrete (ACI 318-02) and Commentary (318R–02). American Concrete Institute, Farmington Hills, Mich.; 2002. 443pp.

[42] Kuo WW, Cheng TJ, Hwang SJ. Force transfer mechanism and shear strength of reinforced concrete beams. Eng Struct 2010;32:1537–46.

[43] He Z, Liu Z, Ma ZJ. Investigation of load-transfer mechanisms in deep beams and corbels. ACI Struct J 2012;109(4):467–76.

[44] Tuchscherer RG, Birrcher DB, Bayrak O. Strut-and-tie model design provisions. PCI J 2011;56(1):155–70.